Article

(Bio)sensing using nanoparticle arrays: on the effect of analyte transport on sensitivity

Nicholas Scott Scott Lynn Jr., and Jiri Homola

Anal. Chem., **Just Accepted Manuscript** • DOI: 10.1021/acs.analchem.6b03002 • Publication Date (Web): 15 Nov 2016

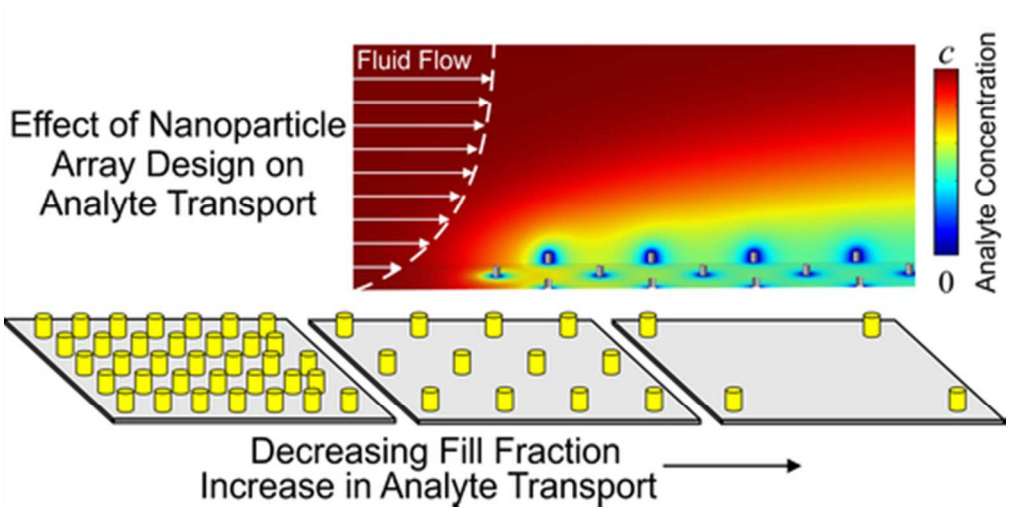

TOC Graphic

42x21mm (300 x 300 DPI)

(Bio)sensing using nanoparticle arrays: on the effect of analyte transport on sensitivity

N. Scott Lynn Jr., Jiří Homola*

Institute of Photonics and Electronics, Academy of Sciences of the Czech Republic
Chaberská 57, Prague, 18251, Czech Republic

*Corresponding Author
Jiří Homola
homola@ufe.cz
Chaberská 57
Prague, Czech Republic

ABSTRACT

There has recently been an extensive amount of work regarding the development of optical, electrical, and mechanical (bio)sensors employing planar arrays of surface bound nanoparticles. The sensor output for these systems is dependent on the rate at which analyte is transported to, and interacts with, each nanoparticle in the array. There has so far been little discussion on the relationship between the design parameters of an array and the interplay of convection, diffusion, and reaction. Moreover, current methods providing such information require extensive computational simulation. Here we demonstrate that the rate of analyte transport to a nanoparticle array can be quantified analytically. We show that such rates are bound by both the rate to a single NP and that to a planar surface (having equivalent size as the array), with the specific rate determined by the fill fraction: the ratio between the total surface area used for biomolecular capture with respect to the entire sensing area. We characterize analyte transport to arrays with respect to changes in numerous parameters relevant to experiment, including variation of the nanoparticle shape and size, packing density, flow conditions, and analyte diffusivity. We also explore how analyte capture is dependent on the kinetic parameters related to an affinity-based biosensor and furthermore, classify the conditions under which the array might be diffusion- or reaction-limited. The results obtained herein are applicable towards the design and optimization of all (bio)sensors based on nanoparticle arrays.

INTRODUCTION

There is currently a growing interest in the use of sensors exploiting the properties of surface-bound nanoparticles (NPs). Across a variety of disciplines, a large number of these sensing applications are based on planar arrays of nanoparticles, where the sensor output is a cumulative average of the signal from the entire array (Fig. 1).[1] The list of electrochemical sensors of this type is quite large and encompasses a variety of transduction (e.g. voltammetric, amperometric, impedometric) and biocomponent mechanisms (e.g. enzymatic- or affinity-based).[2-4] Optically, planar NP arrays are frequently used in surface-enhanced Raman spectroscopy (SERS)[5] and furthermore, form the foundation of affinity-based refractometric biosensors based on the spectroscopy of localized surface plasmons (LSPs), collective resonances (cLSPs), and Fano resonances.[6-8] The list of micromechanical biosensors is smaller in scope, and includes the use of planar arrays of nanocantilevers and nanowires for the affinity-based capture of analyte.[9] Across all mechanisms, a large portion of these sensors are used in a microfluidic flow cell in a *flow-over* format; analysis of sensors based on a *flow-through* approach requires a similar, yet different approach than the one presented herein.[10,11]

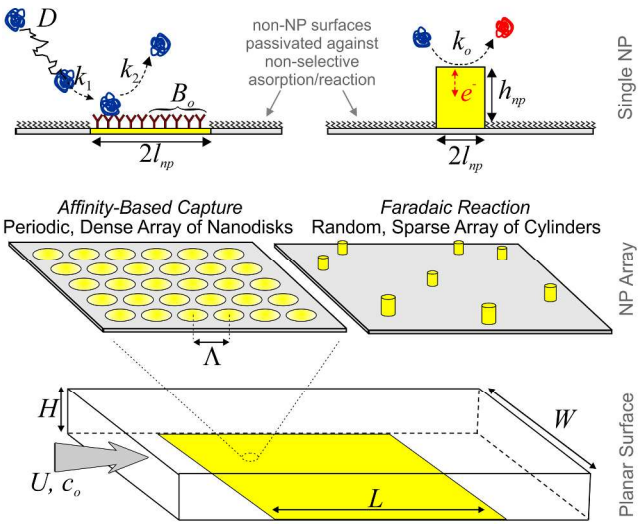

Figure 1. Generalized schematic of a microfluidic sensor based on an array of NPs situated on a microchannel floor.

The performance of a sensor based on an array of NPs is determined through a complex interplay of multiple factors associated with the geometrical design of the array, the conditions to which it is subjected, and a variety of external aspects associated with the transduction mechanism. Nonetheless, the performance of all sensors includes a component dependent on the rate of analyte transport to the sensitive regions of the sensor; this rate is dependent on the parameters shown in Fig. 1 and is independent of the transduction mechanism. Knowledge of how these parameters affect rates of analyte transport is important both for design optimization or in terms of application, to deconvolute (bio)molecular information from a time-series signal.[12,13] This deduction has been commonly accepted in the electrochemical literature;[2,4,14,15] however, discussion within the biophotonics literature is often directed towards the optimization of the array in terms of optical performance, typically in terms of the sensitivity to refractive index (RI) changes. Caution must be used in such an approach: changes to an array with an intent to increase the RI sensitivity might also induce equally detractive (or more) changes in the rate of analyte transport, resulting in a sensor with the same (or worse) detection capability.

Analyte transport to a single NP is a relatively well understood and predictable phenomenon, as it is closely related to analyte transport to a larger, planar surface.[16,17 ,18] The study of analyte transport to an array of NPs is considerably more complex; predictions related to analyte transport in such systems (analytical and numerical) have previously been restricted to pure diffusive transport in symmetric domains.[19-25] There is a relatively miniscule amount of work in the characterization of such arrays when used in a flow environment, where the presence of convection removes the option of a symmetric domain and consequently, the entire length of the array must be considered. Several authors have examined the analogue problem of an array of reactive strips situated orthogonal to the flow direction, thus allowing for a 2D simulation domain;[26,27] however, analytical solutions for that problem have not been developed and furthermore, its relation to the problem considered herein remains unclear. The most beneficial work in this field was recently shown by Shah and Shaqfeh, who provided an elegant characterization of analyte tranport to arrays of disks in simple shear flow, demonstrating that a homogeneous macroscopic boundary condition can be used in place of a heterogeneous microscopic boundary condition for the sensing region.[28] Although useful, this method nonetheless requires the solution of the corresponding differential equations.

In this work we demonstrate an analytical approach to estimate the rate of analyte transport to a planar array of NPs, where said rates are dependent on: (*a*) the fill fraction *f*, defined as the ratio of the total NP surface area used for biomolecular capture with respect to the entire sensing area; (*b*) the rate of mass transfer to a single NP; and (*c*) the rate of mass transfer to a planar surface having equivalent size as the array. Through use of both random walk simulations as well as the theory developed by Shah and Shaqfeh,[28] we show that these analytical expressions remain valid for a wide variety of NP shapes and sizes, array sizes, NP packing densities, flow rates, analyte diffusivities, and kinetic conditions. In addition, we examine the characteristic behavior of a NP array used for the affinity-based collection of analyte for conditions typical to common biosensing experiments.

PROBLEM BACKGROUND AND PARAMETER DEFINITION

Similar to sensors based on either a planar surface[18] or a single NP,[17] analyte transport to an array of NPs can be thought to proceed via two mechanisms, where the rate of convective and diffusive transport from the surrounding fluid to the surfaces of each NP is in balance with the rate of reaction between analyte and said surfaces. Sensors limited exclusively by one mechanism (i.e., where one process occurs at a rate much faster than the other) are termed as being diffusion- or reaction-limited.

Reaction-limited rates of analyte transport are dependent on the specific interaction mechanism between the analyte and NP surface; two such examples are shown in Fig. 1. The list of interaction mechanisms pertinent to this study is vast, hence a quantitative description of each is impractical. Consequently, we limit our discussion to affinity-based biosensors, as this interaction mechanism is ubiquitous among optical and mechanical biosensors and furthermore, is also used in a significant amount of electrochemical NP array biosensors.[2,4] Nevertheless, the results shown herein are applicable to all reaction mechanisms.

Conversely, the diffusion-limited rate of transport to a NP array is independent of both the transduction and interaction mechanism (excluding active analyte transport). Here we quantify these rates as the average analyte flux (J^*, molecules per area per time) to the active regions of the sensor surface (i.e. the NP surfaces).[29] This term is often reported in literature as the mass

transfer coefficient k_m, where by definition $J^* = k_m c_o$, a parameter often used in two compartmental models to extract bioanalytical information from a time-series sensor signal.[30,31] This flux is dependent on many of the parameters shown in Fig. 1, including the height *H* and width *W* of the flow cell, the length *L* of the reactive region, the average fluid velocity *U*, the bulk analyte concentration c_o, the analyte diffusivity *D*, the NP packing density ρ (or pitch Λ, where for square packing $\Lambda = \rho^{-1/2}$), and finally, the surface area A_{np} of a single NP available for analyte interaction (determined by its characteristic length l_{np} and height h_{np}).

Due to its large parameter space, and likewise for purposes of simplicity, we proceed in a dimensionless manner. As discussed below, analyte transport to an NP array is inherently linked with both analyte transport to a planar surface of similar size (defined by *W* and *L*) as well as that to a single NP existing by itself on the sensor floor. We thus define the average dimensionless (steady) *diffusion-limited* flux to a NP array (J_a), to a single NP (J_{np}), and to a planar surface (J_p). These dimensionless values – also known as the Sherwood number – are calculated as $J = J^* H / c_o D$, irrespective of subscript, where J^* represents the dimensional value.

As noted by others,[22,26,28] another key dimensionless parameter for any NP array is the fill fraction $f = A_{np}\rho$. A well-known benefit of miniaturization is that the diffusion-limited flux to a sensor will increase as the characteristic size of the sensing surface decreases;[17,18] it thus follows that J_{np} and J_p set the upper and lower bounds for J_a, specifically in the limits of $f \to 0$ and $f \to 1$, respectively (the same can be said for the dimensional values).

We begin our analysis with an examination of the diffusion-limited analyte transport to both a planar surface and a single NP, including a review (and extension) of previous work involved in the prediction of both J_p and J_{np}. We then demonstrate that those two values can be used to predict J_a under nearly all relevant (bio)sensing conditions. Finally, we extend our discussion to sensors based on an affinity mechanism, including conditions spanning across both the diffusion- and reaction-limited regime.

RESULTS AND DISCUSSION

The numerical data shown here were calculated via two separate methods; details on both can be found in the supporting information. The first method consisted of simulations based on the random walk (RW) method, a technique often used to quantify mass transfer in complex domains,[32] applied here towards arrays having both periodic (square packed) and random order. The second method involved the use of finite element (FE) simulations to model mass transfer to a planar surface having a homogeneous 1st order reactive boundary condition proposed by Shah and Shaqfeh.[28]

Diffusion-Limited Transport to a Planar Surface. As in previous relevant works, we examine the case such that the width of the reactive region spans the entire width of the microchannel, where $W > H$ (Fig. 1).[33] For the problem herein, the relevant dimensionless parameters affecting J_p include the sensor aspect ratio $\eta = L/H$, the channel Peclét number $\mathrm{Pe} = UH/D$, and the sensor Peclét number $\mathrm{Pe}_s = 6\eta^2\mathrm{Pe}$.[34] The latter two values relate the importance of convection vs. diffusion on the scale of the microchannel and the sensing surface, respectively. The majority of microfluidic biosensors are operated under conditions such that Pe > 1.

One trait of diffusion-limited sensors is that the concentration of analyte (in solution) immediate to the active sensor surface (c_s) is often many orders of magnitude below c_o. The analyte boundary (depletion) layer has a thickness δ and a variable shape, the latter of which determines the characteristics of analyte transport. This is shown illustratively in Fig. 2, which plots the conditions leading to similar boundary layer shapes (i.e. phases) for a planar sensor with Pe > 1.

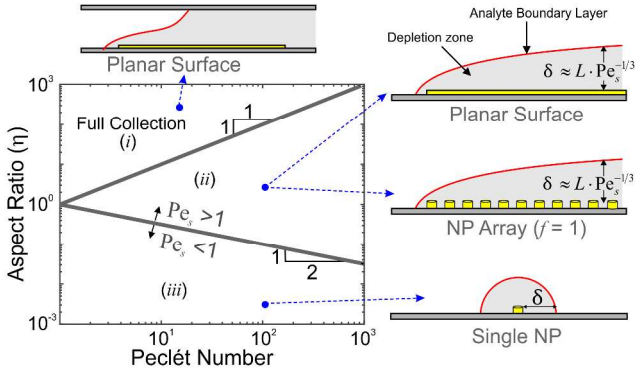

Figure 2. Phase map for the diffusion-limited analyte transport to a planar surface (Pe > 1). Also shown are generalized shapes of the analyte boundary layer for a variety of sensor types in each phase. Sensors operated in phase (*i*), often termed full collection, will interact with all of the analyte flowing past, where the analyte boundary layer spans the entire height of the microchannel. In phase (*ii*) the boundary layer for a planar sensor will be small with respect to both the channel height and the sensor length; transport characteristics will be similar to that of a NP array with $f \approx 1$. In phase (*iii*), the boundary layer will be small with respect to the channel height, but large with respect to the sensor; under most conditions a single NP will exist in this phase (i.e. $\mathrm{Pe}_{np} < 1$).[18]

It remains desirable to predict rates of transport for the entire range of conditions shown in Fig. 2. The dimensionless flux to a planar sensor operated in phase (*i*) can be approximated by $J_p \sim \mathrm{Pe}/\eta$. Using this estimation, the dimensionless flux across all of the phases shown in Fig. 2 can be estimated by

$$J_p^{-\alpha} = \left(\mathrm{Pe}/\eta\right)^{-\alpha} + \left(\mathcal{F}_p/\eta\right)^{-\alpha}, \qquad (1)$$

where α is a constant and is O(1). The term $\mathcal{F}_p = \mathcal{F}_p\left(\mathrm{Pe}_s\right)$ have been the focus of previous studies:[35] an estimate for $\mathcal{F}_p$ under conditions such that $\mathrm{Pe}_s > 1$ was established by Newman[36] as $\mathcal{F}_p = 0.8075\mathrm{Pe}_s^{1/3} + 0.7058\mathrm{Pe}_s^{-1/6} - 0.1984\mathrm{Pe}_s^{-1/3}$; likewise, an estimate under conditions such that $\mathrm{Pe}_s < 1$ was established by Ackerberg[37] as $\mathcal{F}_p = \pi G\left(1 - 0.04633\mathrm{Pe}_s G\right)$, where

$G^{-1} = \ln(4\mathrm{Pe}_s^{-1/2}) + 1.0559$. We have found that a value of $\alpha = 2.5$ provides a sufficient fit to data from 2D FE simulations, demonstrated in the supplementary information (Fig. S-6). For sensors operated under conditions such that $\mathrm{Pe} > 2$ in the range of $10^{-2} < \eta < 10^{2}$, such FE data are within 7% of that given by Eqn. (1).

Diffusion-Limited Transport to a single NP. The diffusion-limited mass transfer to a single NP, and by extension an array of NPs, involves two additional parameters: the NP aspect ratio σ, defined for the NP shapes considered here as $\sigma^2 = A_{np} / \pi H^2$, which relates the size of a NP in terms its surface area to the size of the microchannel; and the NP Peclét number $\mathrm{Pe}_{np} = 6\sigma^2 \mathrm{Pe}$. The parameters σ and Pe_{np} are analogous to η and Pe_s; because of the small size of a NP, most experimental conditions will correspond to $\mathrm{Pe}_{np} < 1$.

In this study we consider mass transfer to several NP shapes commonly found in experiment (disks, hemispheres, pyramids, and cylinders). We show here that estimations of the average flux to the latter three shapes can be obtained with sufficient accuracy by scalar modification of the flux to a disk at equivalent Pe_{np}, i.e., under similar influence of convective vs. diffusive transport on the length scale of the NP. Several of the NP shapes considered herein are associated with multiple characteristic lengths, thus we calculate σ for each NP in terms of A_{np}. This approach follows the example of pure diffusive transport: adjusted for constant surface area the ratio between the steady diffusion-limited flux to a hemisphere vs. that to a disk is $g = \pi\sqrt{2}/4 \sim 1.11$.

The average steady diffusion-limited flux to the NP shapes considered herein can be estimated as

$$J_{np} = \frac{g}{\pi\sigma} \cdot \begin{cases} 2.157\mathrm{Pe}_{np}^{1/3} + 4.037\mathrm{Pe}_{np}^{-1/6} - 1.285\mathrm{Pe}_{np}^{-1/3} & (\mathrm{Pe}_{np} > 0.44) \\ \dfrac{4 - 0.123 \cdot \mathrm{Pe}_{np}{}^{3/2}}{1 - 0.203 \cdot \mathrm{Pe}_{np}{}^{1/2}} & (\mathrm{Pe}_{np} < 0.44) \end{cases}, \qquad (2)$$

where g is a shape factor and is O(1) for NP shapes such that $h_{np} / 2l_{np} \approx 1$, and by definition g = 1 for a disk. The component after the bracket for $\mathrm{Pe}_{np} < 0.44$ is taken directly from the solution

given by Phillips *et al.*,[38] whereas the component for $\mathrm{Pe}_{np} > 0.44$ is a modification of the solution presented by Stone,[39] which allows for improved accuracy in the range of $\mathrm{Pe}_{np} \approx 1$ while maintaining the same leading order term that is accurate for $\mathrm{Pe} >> 1$ (details in the supplementary information). In the supplementary information we show that Eqn. (2) lies within 0.5% of data from FE simulations for the steady diffusion-limited flux to a nanodisk across the range of $10^{-4} < \mathrm{Pe}_{np} < 10^{4}$.

We used the FE method to calculate the dimensionless flux to multiple NP shapes and sizes under conditions of varying Pe_{np}. Figure 3a shows quantitative data from these simulations; the FE data for all of the NP shapes are < 6% from that predicted by Eqn. (2) using the respective values of *g* for each shape (the data for cylinders with $h_{np}/2l_{np} = 1$ are < 11%). The effect of the NP size on the rate of analyte transport is also apparent: it can be seen that at constant Pe_{np} there is an increase in J_{np} with decreases in σ (see also Fig. S-4 in the supplementary information). The qualitative effect of Pe_{np} is shown in Fig. 3b, where analyte contour profiles for all NP shapes have a similar shape and size at equivalent Pe_{np}. This qualitative similarity suggests that the depletion layers for *arrays* of NPs having different NP shapes will be similar, as long as the particles have similar size (i.e. equivalent σ), subject to the same conditions (i.e., equivalent Pe), and are arranged in a similar manner (i.e., equivalent *f*).

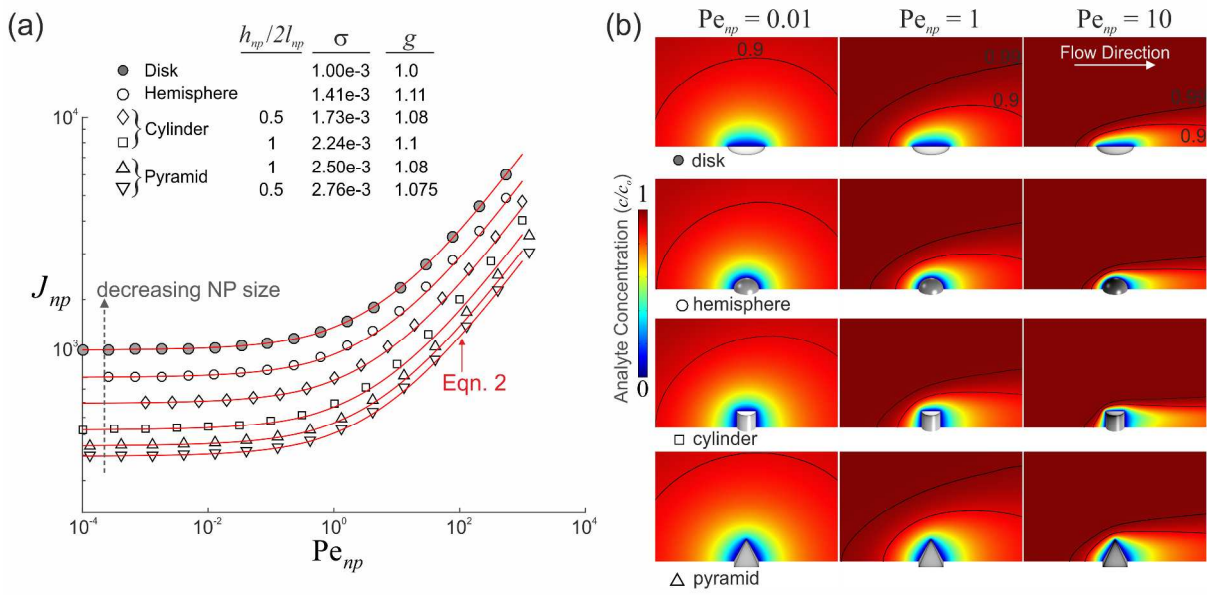

Figure 3. Analyte transport to a single NP (FE simulation data). (a) Dimensionless flux J_{np} as a function of the NP Peclét number for a variety of NP shapes and sizes. The cylinder and pyramid shapes have variable ratio $h_{np}/2l_{np}$. Variation in Pe_{np} for each shape is through changes in Pe. The solid (red) lines represents analytical data taken from Eqn. (2) using respective values of σ and g. (b) Steady-state diffusion-limited analyte concentration profiles (plotted as c/c_o) for several NP shapes for varying Pe_{np}. The black lines represent lines of constant c/c_o (0.9, 0.99).

Diffusion-Limited Transport to a NP Array. Here we show that the diffusion-limited transport to an NP array can be described in terms of J_{np}, J_p, and f. Figure 4 shows data from numerical simulations regarding the diffusion-limited transport to an array of nanodisks under conditions relevant to phase (*ii*) (Fig. 2, where the size of the array is characterized by η), as these conditions represent those most commonly found in experiment.[18] This data demonstrate how the average flux to an array of nanodisks is dependent on the size of the disk, the size of the sensing region, the fill fraction, and the packing order. There is good agreement between the RW and FE data in the results shown in Fig. 4; considering the differences in the numerical

approaches between the RW and FE methods, this agreement serves as a partial verification of both methods.

We propose a phenomenological model to predict J_a that is dependent only on J_{np}, J_p, and f:

$$J_a = \left(\frac{1}{J_{np} - J_p} + \frac{f}{J_p(1-f)} \right)^{-1} + J_p \quad . \tag{3}$$

For periodically packed nanodisks, the difference between the RW and FE data and those predicted by Eqn. (3) are < 6% for all of the data shown in Fig. 4. The flux to arrays with random packing is slightly lower than that to a periodic structure, previously observed via numerical simulation,[28] where the difference between the RW data and Eqn. (3) were <10%.

All of the data shown in Fig. 4 follow a general trend such that as $f \to 1$, the flux to the array asymptotically approach a rate defined by $J_a = J_p f^{-1}$.[40] This behavior will exist only under conditions relevant to phase (*ii*), where deviations from this scaling behavior occur at a critical fill fraction of $f_c \approx J_p / (J_p + 0.1 J_{np})$, shown in Fig. 4b as the red arrows. This scaling relationship is important for sensing applications where the absolute rate of analyte interaction is important (e.g voltammetric or amperometric): for $f > f_c$ the rate of analyte delivery (molecules per time) to an NP array will be equivalent to that of a planar sensor.

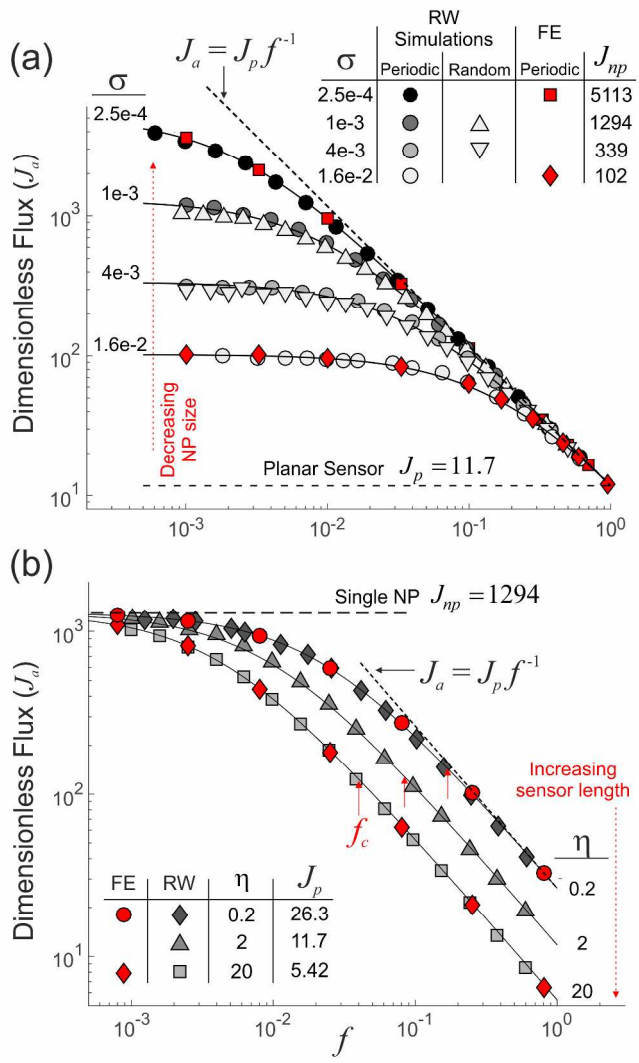

Figure 4. Average diffusion-limited dimensionless flux to a nanodisk array vs. the fill fraction (Pe = 10^3) for a sensor with (a) varying nanodisk size ($\eta = 2$) and (b) varying length of the sensing region ($\sigma = 10^{-3}$). The symbols were numerically calculated via either the FE or RW method. The RW data consist of nanodisk arrays with both periodic and random packing. The solid lines were calculated via Eqn. (3) using the respective values of J_p and J_{np} shown in each figure, which were calculated via Eqn. (1) and (2), respectively.

To demonstrate the accuracy of Eqn. (3) for all of the conditions shown in Fig. 2 (i.e. all conditions that might be expected in experiment), we used FE simulations with the boundary condition proposed by Shah and Shaqfeh[28] to calculate J_a to arrays of periodic nanodisks for sensors with varying f and η in the range of Pe > 1. The data from these simulations are shown in Fig. 5. It can be seen that there is a good match between the numerical and analytical data: for Pe > 2 the numerical data is within 10% of that predicted by Eqns. (1)-(3). In addition, in the supplementary information we show that Eqn. (3) can also be used to estimate the analyte flux to an array of nanostrips (Fig. S-5).

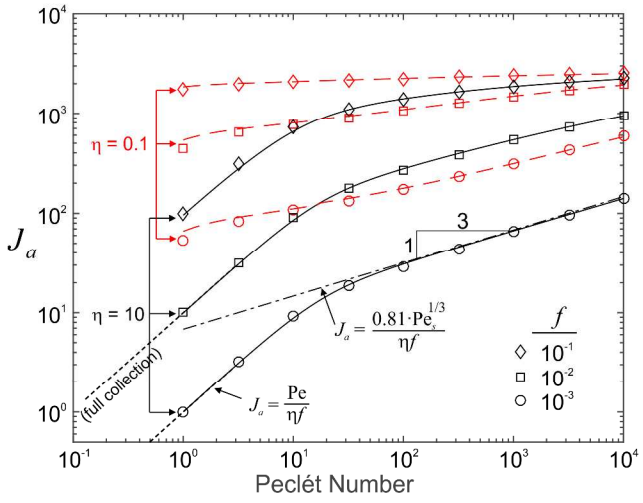

Figure 5. Comparison of FE (symbols) analytical data regarding the diffusion-limited flux to an array of nanodisks having two different sensing region sizes and three different fill fractions ($\sigma = 5\times10^{-4}$). The dotted-dashed line, representing phase (*ii*) behavior, was calculated via the 1st component of the solution presented by Newman,[36] divided by f. The dashed lines represents the limit of full collection (i.e. phase (*i*)), calculated via

$J_a = \mathrm{Pe}/\eta f$. The solid (black, η = 10) and dashed (red, η = 0.1) lines were calculated via Eqn. (3), using Eqns. (1) and (2) for the calculation of J_p and J_{np}, respectively.

Affinity-Based Biosensing with a NP Array. In this section we show that Eqns. (1)-(3) can be used to estimate the quasi-steady collection flux of analyte by an NP array operated via an affinity mechanism, regardless of the kinetic regime (i.e. under diffusion- or reaction-limitations). For such a mechanism, the interaction between analyte and biorecognition element is often described using a 1st order ligand-receptor model, whereby the reactive flux of analyte follows

$$j_R^* = \frac{\partial \beta}{\partial t} = k_1 c_s (B_o - \beta) - k_2 \beta \ , \qquad (4)$$

where β is the surface concentration of captured analyte, k_1 and k_2 are the forward (association) and reverse (dissociation) rate constants, B_o is the surface concentration of biorecognition elements, and c_s is the concentration of analyte at the bioactive surface. In the initial stages of an assay ($\beta \approx 0$) the reactive flux to the system can be approximated by $j_R^* \approx k_1 c_s B_o$. This reactive flux is maximized when $c_s \to c_o$, i.e. under reaction-limited conditions, where it follows that the dimensionless reaction-limited flux can be estimated by $j_R = k_1 B_o H/D$.

To ascertain if a sensor will exist in the diffusion- or reaction-limited regime and furthermore, estimate rates of analyte transport, it is useful to calculate the Damköhler number (Da). This value represents the ratio of reactive capture to the rate of transport of an analyte to the sensor surface; $\mathrm{Da} >> 1$ implies that the system is in the diffusion-limited regime, and $\mathrm{Da} << 1$ implies that the system is reaction-limited. It follows that there are three Damköhler numbers pertinent to sensing with NP arrays: one for the entire array ($\mathrm{Da}_a = j_R/J_a$), for a planar sensor ($\mathrm{Da}_p = j_R/J_p$), and for a single NP ($\mathrm{Da}_{np} = j_R/J_{np}$). Although these expressions follow the definition of the Damköhler number, they can also be derived with an assumption that c_s is homogenous along each (respective) surface, where $c_s/c_o \sim (1+\mathrm{Da})^{-1}$.[18]

The dimensionless fluxes calculated under pure diffusion- ((Eqns. (1)-(3)) or reaction-limitations (defined by j_R) represent the inverse of the resistance of mass transfer, where the sum of diffusion- and reaction-limited resistances represents the total resistance of mass transfer.[28,41,42] It follows that estimations for the quasi-steady dimensionless flux to an array (j_a), a single NP (j_{np}), and a planar surface (j_p) follow

$$j_a = \frac{j_R}{1+\mathrm{Da}_a},\ j_{np} = \frac{j_R}{1+\mathrm{Da}_{np}},\ j_p = \frac{j_R}{1+\mathrm{Da}_p}. \quad (5)$$

These values can be made dimensionless in the same manner as their diffusion-limited counterparts, where $j = j^* H / c_o D$, irrespective of subscript, and j^* represents the dimensional value.

We demonstrate the accuracy of Eqn. (5) in the supplementary information (Figs. S-4, S-5, S-6) through comparison of the analytical calculation of j_p and j_{np} with data taken from FE simulations over a wide range of conditions. In addition, we show that Eqn. (5) also provides a good match to FE solutions regarding the affinity-based analyte collection by an array of nanostrips with variable Da_a (Fig. S-7). Considering these agreements, it is a safe assumption that Eqn. 5 represents a valid method for the estimation of the average flux to an NP array for all values of Da_a.

We illustrate the complex behavior of an affinity-based NP array sensor through the calculation of j_a / j_p across a wide range of conditions common to biosensing experiments. From an experimental perspective, j_a / j_p will be manifested as the ratio in binding rates for a sensor based on a NP array and that based on a planar surface (normalized for similar sensitivity to β). The convenience of this ratio is due to the significant amount of literature on planar biosensors, from both a transduction and mass transfer point of view.

Figure 6 plots j_a / j_p for two nanodisk arrays (f = 0.1, 0.01) as a function of the analyte diffusivity and the association rate constant. This figure provides insight into the characteristic behavior of analyte collection by a NP array, which can be separated into two general regimes.

The first regime regards reaction-limited conditions for both formats (i.e. $\mathrm{Da}_{np} < \mathrm{Da}_p < 1$), where respective rates of transport will be equivalent and $j_a/j_p \to 1$. The second regime is represented by the conditions such that $\mathrm{Da}_p > 1$, where as expected, j_a/j_p is higher for the array with a lower fill fraction (constant k_1 and D). Increases in k_1 (at constant D) lead to monotonic increases in j_a/j_p; this increase is asymptotic as analyte transport to a single NP becomes diffusion-limited, where the transition to said regime is faster for analytes having lower diffusivities. The effect of variable diffusivity (at constant k_1) on the enhancement is more complicated: there is a local maximum at a diffusivity corresponding to a value of $\mathrm{Da}_{np} \approx 1$, which can be explained via scaling analysis (supplementary information).

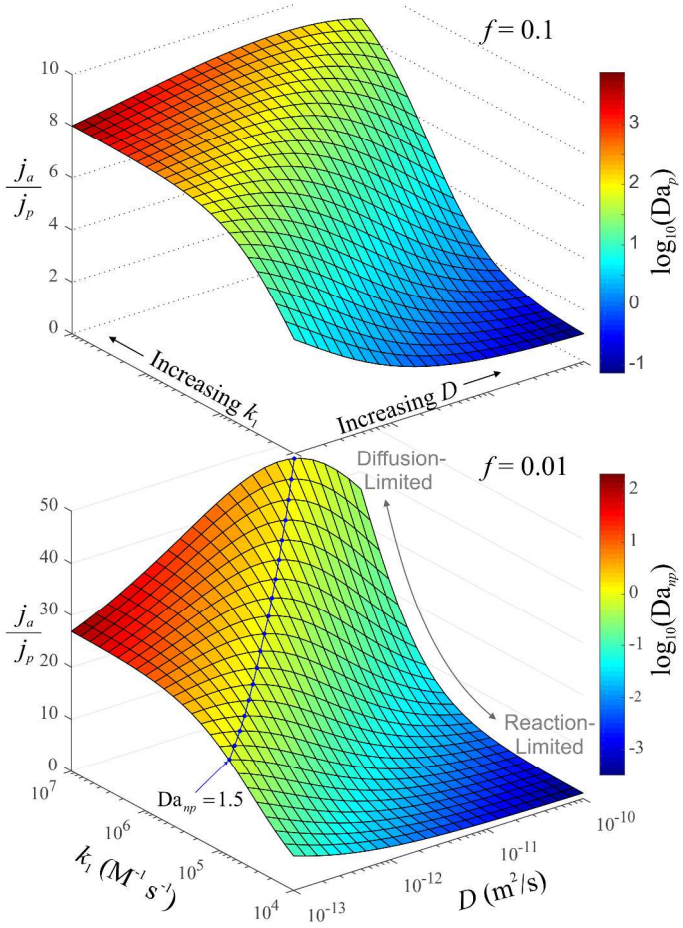

Figure 6. Ratio j_a / j_p of the quasi-steady, affinity-based analyte collection flux between a nanodisk array and that of a planar sensor (η = 20, σ = 10-3, l_{np} = 50 nm, H = 50 μm, U = 2 mm/s, L = 1 mm, and $B_o = 8\times10^{-14}$ mol mm^{-2}). The color map pertains to Da_p (top, f = 0.1) and Da_{np} (bottom, f = 0.01). These data were calculated via Eqn. (5), using Eqns. (1) -(3) for the calculation of J_p, J_{np}, and J_a, respectively.

The results shown in Fig. 6 highlight the importance of the contribution of analyte transport to the sensor response for NP arrays operated through an affinity-based mechanism: using the same NP array, experiments based on two different biorecognition element/analyte pairs can lead to a sensor response that might vary by more than an order of magnitude with respect to the sensor response obtained from a planar sensor (e.g. used for purposes of comparison).

Final Notes, and Applicability to Other Fields. As should be required from all results derived from simulation, the experimental verification of the expressions proposed herein – specifically Eqn. (3) and by extension, Eqn. (5) – has not been established and remains the focus of current research. Nevertheless, we have demonstrated that the analyte transport to an array of NPs is linked with both that to a planar surface and that to a single NP; analytical solutions for the latter two (represented by Eqns. (1) and (2)) have been accepted, and in many cases verified, within the mass and heat transfer literature.[17,18] In addition, we have demonstrated a clear link between the problem herein and the analogous problem of flow over an array of orthogonally situated sensing regions. As with their planar counterparts, however, a comprehensive discussion on the transport behavior of sensors based on NP arrays lies well outside what is possible in a single article.

The use of the equations herein follows a logical progression: the values shown in Fig. 1 can be used to calculate relevant dimensionless parameters (η, σ, Pe_s, Pe_{np}, and f), which can then be used directly in Eqns. (1)-(3) to calculate J_a. The use of such information for purposes of design or optimization will eventually depend on both the transduction and interaction mechanism of the sensor under consideration. For example, the kinetic parameters k_1 and B_o can be used with Eqn. (5) to predict how analyte transport will be affected by potential changes

to an array (e.g. changes in ρ, l_{np}, L, etc.) operated using an affinity-mechanism; such information can be compared to how those same changes affect other parameters related to the sensor sensitivity (e.g. the sensitivity to RI changes). If desired, dimensional values for the analyte collection flux can be obtained as $j_a^* = j_a c_o D/H$. Similarly, the (dimensional) mass transfer coefficient can be calculated as $k_m = J_a D/H$, knowledge of which can be used for purposes of kinetic analysis.

It is important to note that the equations used herein represent the steady-state (for diffusion-limited behavior) or in the case of an affinity-based sensor, the quasi-steady values for the analyte flux. The conditions under which an experimental system can be considered to be steady follow the discussion of Squires *et al.*:[18] for diffusion-limited systems the time scale for the analyte boundary layer to form will be on the order of $\tau_\delta \sim \delta^2/D$. Although the discussion here did not focus on the size of δ for a NP array, one can estimate its maximum size by using the estimations for that of a planar sensor, thus providing an upper limit for τ_δ. The boundary layer sizes for such planar sensors can be estimated by $\delta \sim LPe_s^{-1/3}$ and $\delta \sim LPe_s^{-1/2}$ for $Pe_s >> 1$ and $Pe_s << 1$, respectively.[18] An upper limit on the conditions of when the sensor can be considered to be quasi-steady follows a similar argument.

In addition to sensing applications, these results are applicable to other fields, for example, the use of NP arrays for the promotion of electrocatalytic reactions. It has been shown that the diffusion-limited current (related to the rate of reactant transport) for such arrays can affect the selectivity and distribution of products.[43,44] Furthermore, in such systems there also exists a balance between diffusion- and reaction-limited conditions, where the boundary between the two regimes (as a function of *f*) remain unknown. The results shown here can be used to elucidate such information.

CONCLUSIONS

The topic of analyte transport to a NP array is inherently complex and is dependent on a multitude of factors. Despite this complexity, we have demonstrated that the steady-state analyte

transport to such an array can be suitably quantified through a series of analytical expressions that account for a wide range of NP shapes, sizes, packing densities, array sizes, operating conditions, and in the case of an affinity-based biosensor, analyte/bioreceptor systems. This work makes it evident that when using such arrays for purposes of detection, or likewise to obtain (bio)molecular information, attention must be given to how the design of the NP array affect *both* the sensitivity of transduction as well as the characteristics of analyte transport. We have established and, through comparison with numerical simulation, verified analytical equations that provide estimations for such rates of analyte transport. We believe that the most valuable aspect of this work not in the precision of the equations shown herein, but in the use of such equations as a tool towards the design of NP array based sensors; for example, they can provide information on how the sensor response might scale with either changes to the parameters directly related to the array or equally important, changes to the sensing conditions the array is subjected to.

ACKNOWLEDGMENT

This work was supported by both the Praemium Academiae of the Academy of Sciences of the Czech Republic as well as the Czech Science Foundation (contract # P205/12/G118).

REFERENCES

(1) Shipway, A. N.; Katz, E.; Willner, I. *Chemphyschem* **2000**, *1*, 18-52.
(2) Ongaro, M.; Ugo, P. *Anal Bioanal Chem* **2013**, *405*, 3715-3729.
(3) Singh, P. S. *Access, IEEE* **2015**, *3*, 249-259.
(4) Dawson, K.; O'Riordan, A. *Annual Review of Analytical Chemistry, Vol 7* **2014**, *7*, 163-+.
(5) Luo, S. C.; Sivashanmugan, K.; Liao, J. D.; Yao, C. K.; Peng, H. C. *Biosensors & Bioelectronics* **2014**, *61*, 232-240.
(6) Dahlin, A. B.; Wittenberg, N. J.; Hook, F.; Oh, S. H. *Nanophotonics-Berlin* **2013**, *2*, 83-101.
(7) Estevez, M. C.; Otte, M. A.; Sepulveda, B.; Lechuga, L. M. *Anal Chim Acta* **2014**, *806*, 55-73.
(8) Stewart, M. E.; Anderton, C. R.; Thompson, L. B.; Maria, J.; Gray, S. K.; Rogers, J. A.; Nuzzo, R. G. *Chem Rev* **2008**, *108*, 494-521.
(9) Arlett, J. L.; Myers, E. B.; Roukes, M. L. *Nat Nanotechnol* **2011**, *6*, 203-215.
(10) Escobedo, C.; Brolo, A. G.; Gordon, R.; Sinton, D. *Analytical Chemistry* **2010**, *82*, 10015-10020.
(11) Eftekhari, F.; Escobedo, C.; Ferreira, J.; Duan, X. B.; Girotto, E. M.; Brolo, A. G.; Gordon, R.; Sinton, D. *Analytical Chemistry* **2009**, *81*, 4308-4311.
(12) Arrigan, D. W. M. *Analyst* **2004**, *129*, 1157-1165.
(13) Mason, T.; Pineda, A. R.; Wofsy, C.; Goldstein, B. *Math Biosci* **1999**, *159*, 123-144.

(14) Gaster, R. S.; Xu, L.; Han, S. J.; Wilson, R. J.; Hall, D. A.; Osterfeld, S. J.; Yu, H.; Wang, S. X. *Nat Nanotechnol* **2011**, *6*, 314-320.
(15) Duan, X. X.; Li, Y.; Rajan, N. K.; Routenberg, D. A.; Modis, Y.; Reed, M. A. *Nat Nanotechnol* **2012**, *7*, 401-407.
(16) Dahlin, A. B. *Sensors-Basel* **2012**, *12*, 3018-3036.
(17) Sheehan, P. E.; Whitman, L. J. *Nano Lett* **2005**, *5*, 803-807.
(18) Squires, T. M.; Messinger, R. J.; Manalis, S. R. *Nature Biotechnology* **2008**, *26*, 417-426.
(19) Davies, T. J.; Compton, R. G. *J Electroanal Chem* **2005**, *585*, 63-82.
(20) Godino, N.; Borrise, X.; Munoz, F. X.; del Campo, F. J.; Compton, R. G. *Journal of Physical Chemistry C* **2009**, *113*, 11119-11125.
(21) Lucas, S. K.; Sipcic, R.; Stone, H. A. *Siam J Appl Math* **1997**, *57*, 1615-1638.
(22) Bishop, J.; Chagovetz, A.; Blair, S. *Nanotechnology* **2006**, *17*, 2442-2448.
(23) Guo, J. D.; Lindner, E. *Analytical Chemistry* **2009**, *81*, 130-138.
(24) Nagy, G.; Denuault, G. *J Electroanal Chem* **1997**, *433*, 175-180.
(25) Henstridge, M. C.; Compton, R. G. *Chem Rec* **2012**, *12*, 63-71.
(26) Juhasz, N. M.; Deen, W. M. *Ind Eng Chem Res* **1991**, *30*, 556-562.
(27) Abolfath-Beygi, M.; Krishnamurthy, V.; Cornell, B. *Ieee Sens J* **2013**, *13*, 1265-1273.
(28) Shah, P. N.; Shaqfeh, E. S. G. *J Fluid Mech* **2015**, *782*, 260-299.
(29) The importance of the flux, as opposed to the rate of analyte delivery (molecules per time), stems from the fact that the sensitivity of many transduction mechanisms (e.g. refractometric, impedometric) is proportional to the surface density of analyte and thus directly proportional to the flux.
(30) Myszka, D. G.; He, X.; Dembo, M.; Morton, T. A.; Goldstein, B. *Biophys J* **1998**, *75*, 583-594.
(31) Myszka, D. G.; Morton, T. A.; Doyle, M. L.; Chaiken, I. M. *Biophys Chem* **1997**, *64*, 127-137.
(32) Salamon, P.; Fernandez-Garcia, D.; Gomez-Hernandez, J. J. *Water Resour Res* **2006**, *42*.
(33) For sensors such that the reactive surface does not span the entire width of the channel (e.g. a circular region on the microchannel floor), Eqn. (2) is more appropriate for the calculation of Jp (via substitution of Pes with Penp).
(34) The value 6 in Pes is a result of the parabolic flow profile in a (sufficiently wide) microchannel, where the shear rate at the sensor surface is 6*U/H.
(35) This term represents the dimensionless flux using L as the characteristic length.
(36) Newman, J. *Electroanalytical Chemistry* **1973**, *6*, 279-297.
(37) Ackerberg, R. C.; Patel, R. D.; Gupta, S. K. *J Fluid Mech* **1978**, *86*, 49-65.
(38) Phillips, C. G. *Q J Mech Appl Math* **1990**, *43*, 135-155.
(39) Stone, H. A. *Phys Fluids a-Fluid* **1989**, *1*, 1111-1122.
(40) This relationship is derivable via scaling analysis for arrays under conditions relevant to phase (ii)
(41) Bartholomew, C. H.; Farrauto, R. J. *Fundamentals of industrial catalytic processes*; John Wiley & Sons, 2011.
(42) Roberts, G. W. *Catalysis in organic synthesis* **2012**, 1.
(43) Wickman, B.; Seidel, Y. E.; Jusys, Z.; Kasemo, B.; Behm, R. J. *Acs Nano* **2011**, *5*, 2547-2558.
(44) Seidel, Y. E.; Schneider, A.; Jusys, Z.; Wickman, B.; Kasemo, B.; Behm, R. J. *Faraday Discuss* **2008**, *140*, 167-184.